Applied Physics Letters

RESEARCH ARTICLE | JANUARY 28 2025

Weak coupling of buckled germanene with high Fermi velocity on semiconducting Cu_2Te

Bo Li; Zhen Jiao; Ping Li; Yanlin Tao; Qin Liao; Shicheng Xu; Qiwei Tian; Chen Zhang;
Li Zhang; Yuan Tian; Long-Jing Yin; Lijie Zhang; Zhihui Qin ✉

Appl. Phys. Lett. 126, 041903 (2025)
https://doi.org/10.1063/5.0249308

Applied Physics Letters ARTICLE pubs.aip.org/aip/apl

Weak coupling of buckled germanene with high Fermi velocity on semiconducting Cu_2Te

Cite as: Appl. Phys. Lett. **126**, 041903 (2025); doi: 10.1063/5.0249308
Submitted: 17 November 2024 · Accepted: 11 January 2025 ·
Published Online: 28 January 2025

Bo Li,[1] Zhen Jiao,[2,3] Ping Li,[4] Yanlin Tao,[1] Qin Liao,[1] Shicheng Xu,[1] Qiwei Tian,[1] Chen Zhang,[1] Li Zhang,[1] Yuan Tian,[1] Long-Jing Yin,[1] Lijie Zhang,[1] and Zhihui Qin[1,a)]

AFFILIATIONS

[1] Key Laboratory for Micro/Nano Optoelectronic Devices of Ministry of Education & Hunan Provincial Key Laboratory of Low-Dimensional Structural Physics and Devices, School of Physics and Electronics, Hunan University, Changsha 410082, People's Republic of China
[2] Bond and Band Engineering Group, School of Physical Science and Technology, Southwest Jiaotong University, Chengdu 610031, People's Republic of China
[3] State Key Laboratory of Silicon and Advanced Semiconductor Materials, Zhejiang University, Hangzhou 310027, People's Republic of China
[4] State Key Laboratory for Mechanical Behavior of Materials, Center for Spintronics and Quantum Systems, School of Materials Science and Engineering, Xi'an Jiaotong University, Xi'an, Shaanxi 710049, People's Republic of China

[a)] Author to whom correspondence should be addressed: zhqin@hnu.edu.cn

ABSTRACT

Despite its promise, growing a quasi-freestanding monolayer of germanene with Dirac cone signature remains a significant attention. Synthesizing germanene on semiconductor surfaces is highly desirable to preserve its linear energy dispersion near the K points, which has been experimentally challenging. Here, we report the molecular beam epitaxy of monolayer germanene on semiconducting Cu_2Te supported by Cu(111). Scanning tunneling microscopy/spectroscopy (STM) revealed a low-buckled honeycomb lattice of germanene, exhibiting an intrinsic Dirac cone at the K point. By combining STM measurements with theoretical simulations, we confirm that germanene atoms occupy threefold hollow sites on Cu_2Te via van der Waals interaction. Remarkably, by dI/dV spectra fitting, we find the prepared germanene owns the Fermi velocity of $(6.9 \pm 0.1) \times 10^5$ m/s, which is slightly higher than the density functional theory calculated 4.6×10^5 m/s with considering the dielectric constant of the underlying Cu_2Te, implying the weak coupling of germanene with the substrate. This work provides a platform for further exploring the ballistic charge transport properties of germanene with a Dirac cone.

The successful isolation of graphene, the first two-dimensional (2D) material, has sparked a wave of groundbreaking research in the realm of 2D materials and their heterostructures, revealing exciting physics and opening doors for diverse applications.[1,2] Over the past two decades, 2D materials and their heterostructures have provided platforms of exotic physical property explorations and potential technological advancements.[3–5] Among them, germanene is a single layer of germanium atoms arranged in honeycomb lattice, which has attracted significant attention.[6] In contrast to carbon, the lowest energy structure of germanium is not the graphite-like sp^2 structure, but rather the diamond sp^3 bulk structure. However, theoretical calculations find that a freestanding sp^3 hybridized germanium layer is unstable due to phonon instabilities. As a result, germanene adopts a mixed sp^2–sp^3 hybridization. Therefore, the two atoms in a primitive cell of freestanding germanene are not in the same plane, but are slightly buckled. This special feature opens a door for germanene to be functionalized and bandgap tuned.[7–9] Despite the buckling, germanene can still preserve the Dirac cone at the K point of the Brillouin zone. Furthermore, the significant stronger spin–orbit coupling in germanene compared to graphene gives rise to the observation of quantum spin Hall (QSH) effect experimentally.[10,11]

In the past decade, germanene has been reported to synthesize on variable metal surfaces;[12–19] however, its intriguing physical properties are annihilated due to the strong interaction between the metal substrate and germanene. There are quite limited reports on the growth of germanene on nonmetallic surfaces,[8,20,21] which are crucial for preserving its intrinsic properties.

In this work, we report the growth of a quasi-freestanding monolayer of germanene with a low-buckled honeycomb structure and Dirac cone signature on a delicately selected Cu_2Te buffer layer by molecular beam epitaxy (MBE). Combining scanning tunneling microscopy/spectroscopy (STM/STS) measurements with first-principles calculations confirms the van der Waals interaction of germanene with the semiconducting substrate by occupying the hollow position of Cu_2Te. Remarkably, the weak coupling between germanene and the substrate results in the linear band structure in the bandgap region of the Cu_2Te substrate. From experimental *dI/dV* spectra fitting, the prepared germanene monolayer has high Fermi velocity of $(6.9 \pm 0.1) \times 10^5$ m/s, slightly higher than the density functional theory (DFT) calculated to be 4.6×10^5 m/s considering the dielectric constant of the underlying Cu_2Te, implying the weak coupling of germanene with the substrate. These findings render the buckled germanene on semiconducting substrate a promising material for exploring the "Dirac physics" properties.

The experiments were carried out at a home-built ultrahigh-vacuum (UHV)-MBE chamber equipped with an STM (Unisoku Co. Ltd.). The base pressure of the system was below 1×10^{-10} Torr. Mechanically cut Pt/Ir (80/20) tips were used for imaging and spectroscopy. Prior to the growth, the Cu(111) substrate was cleaned by multiple circles of sputtering (800 eV) and annealing (∼850 K, 10 min). Subsequently, Te atoms (99.999%, Alfa Aesar) were thermally evaporated onto the Cu(111) substrate held at room temperature. Cu_2Te_2 and Cu_2Te were obtained by post annealing both at ∼650 K for 10 min. The germanium (99.9999%, Alfa Aesar) was heated at 880 °C from a commercial Knudsen cell and evaporated onto Cu_2Te_2 and Cu_2Te held at ∼570 K. The STM measurements were performed at room temperature (RT). Differential conductivity (*dI/dV*) was measured using a standard lock-in amplifier with a modulating signal of 50 mV and 773 Hz. The system were carefully calibrated by Si(111)–(7 × 7) and Au(111) surface. All the data processes were conducted by the free software WSxM.[22]

We employed the Vienna *ab initio* simulation package (VASP) for the first-principles calculations based on density functional theory (DFT). General gradient approximation (GGA) in the form of Perdew−Burke−Ernzerhof functional was adopted for the exchange−correlation functional.[23] The van der Waals density functional (DFT-D_3) was capable of treating the dispersion force.[24] The energy convergence value between two consecutive steps was chosen as 10^{-6} eV. The Hellman–Feynman forces are taken to be converged when they become smaller than 0.01 eV/Å. The plane wave basis set used a kinetic energy cutoff of 500 eV. The substrate was simulated by the slab model consisting of three layers of Cu(111) and one layer of Cu_2Te. The lattice constant of Cu_2Te was selected as the experimental values 4.50 Å. A 20-Å-thick vacuum slab was considered to avoid the interactions between the supercells in the nonperiodic direction. A mesh of 12 × 12 × 1 Γ-centered Monkhorst–Pack was used to sample the Brillouin zone of the supercells.[25] The germanene structures with (2 × 2) periodicity were deposited on the $\sqrt{3}\times\sqrt{3}$ Cu_2Te substrate in the simulation.

To obtain the epitaxial freestanding germanene monolayer on nonmetallic surface, the choice of the substrate or surface modification is crucial. In this study, Cu(111) single crystal with buffer layer (Cu_2Te or Cu_2Te_2) were selected to grow monolayer germanene under ultrahigh-vacuum conditions. Before further investigating the epitaxial growth of monolayer germanene, we briefly check the crystal structure of the buffer layer. Previous studies have demonstrated that the surface structure of tellurium deposited on Cu(111) varies as a function of Te coverage.[26,27] At low coverage [1/3 monolayer (ML)], an ordered $(2\sqrt{3} \times 2\sqrt{3})R30^\circ$ superstructure, i.e., "stripe" phase, is formed in terms of Cu_2Te_2 adsorbate chains.[26] When the Te coverage exceeds 1.5 ML, a two-dimensional flat Cu_2Te surface forms.[27–30]

In our experiments, after the deposition of 1.2 ML of Te atoms onto Cu(111) and subsequent annealing at ∼650 K for 10 min, the randomly distributed stripe phase of Cu_2Te_2 is formed [see Fig. 1(a)]. Note that the brighter contrast regions in Fig. S1 of the supplementary material correspond to the bilayer Cu_2Te_2. As plotted in Figs. S1(c) and S1(d), the measured step heights indicate an interlayer distance of approximately 3.0 Å. The atomically resolved STM images of Fig. 1(b) clearly present the topmost Te atoms in the Cu_2Te_2 monolayer, exhibiting a single stripe with a periodicity of ∼0.40 nm along the chain [Figs. 1(b) and 1(c)]. The corresponding fast Fourier transform (FFT) shown in inset confirms a lattice constant of ∼0.40 nm [Fig. 1(b)]. Furthermore, the *dI/dV* spectrum, which is proportional to the local density of states (LDOS), shows metallic characteristics [Fig. 1(d)]. These results are consistent with the previous findings.[26,27]

Further deposition of 2 ML Te and subsequent annealing at ∼650 K for 10 min led to the formation of flat Cu_2Te film [Fig. 1(e)]. The enlarged STM image demonstrates a close-packed hexagonal arrangement of surface protrusions with a periodicity of ∼0.45 nm, forming a threefold symmetric hexagonal lattice confirmed by its FFT [see Fig. 1(f) and its inset]. The distinct electronic properties of the Cu_2Te structure are also reflected in the *dI/dV* spectrum, where a pronounced ∼0.3 eV bandgap is observed [see Fig. 1(h) and the inset], confirming that Cu_2Te is a narrow bandgap semiconductor. This bandgap is slightly smaller than that previous report by ARPES and DFT,[29] which can be attributed to the hybridizing with the Cu(111) substrate. More experimental data for the Cu_2Te semiconductor can be found in the supplementary material.

The growth of germanene is highly dependent on the deposition condition and the interactions with epitaxial substrates. To monitor the epitaxial process, STM was well employed to capture large-scale topographies and atomic resolution images, respectively. Intriguingly, as illustrated in the epitaxial growth diagram [Fig. 1(i)], we found distinct growth behavior of germanium on Cu_2Te and Cu_2Te_2 substrates both held at ∼570 K under UHV condition. As shown in Figs. 1(j) and 1(k), STM topographies reveal that germanium forms numerous flat islands on Cu_2Te, whereas forming condensed clusters adsorbing on Cu_2Te_2, suggesting that Cu_2Te is more conducive to the growth of germanene.

From the STM image shown in Fig. 1(l), a two-dimensional growth mode is observed at the initial stages, with many uniform and continuous triangle and hexagon germanium islands forming across the surface of Cu_2Te. The STM topographic image reveals flattop islands with terrace step height of ∼0.37 Å, suggesting a van der Waals distance between the monolayer island and Cu_2Te substrate with a weak coupling. These epitaxial monolayer germanium islands are expected to host the quasi-freestanding electronic structures. Additional data of the resulting film with lateral sizes of ∼90 nm can be found in Fig. S3.

To gain more information of the surface, we investigated the structural and electronic properties of the germanium films in detail.

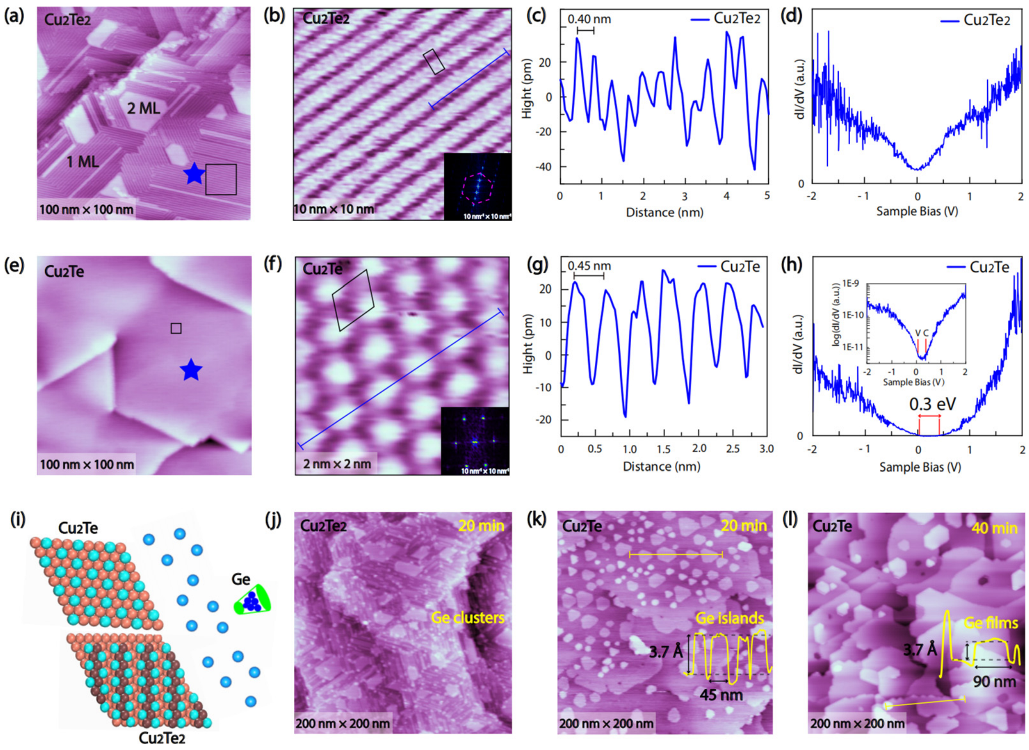

FIG. 1. (a) Large-scale STM topographic image ($V_{bias} = 1$ V, I = 100 pA) of coexisting with the first/second layer Cu_2Te_2. (b) Zoom-in STM image ($V_{bias} = 1$ V, I = 100 pA) of "stripe" phase Cu_2Te_2. Inset: the 2D FFT of the STM image. (c) Line profile along the blue line marked in (b), revealing the periodicity of the synthesized Cu_2Te_2 is ∼0.4 nm. (d) The *dI/dV* spectrum (Setpoint: $V_{bias} = 0.6$ V, I = 80 pA) of Cu_2Te_2 marked in (a), revealing metallic characteristic. (e) Large-scale STM topographic image ($V_{bias} = 0.6$ V, I = 80 pA) of Cu_2Te substrate. (f) Atomic resolution STM image ($V_{bias} = 0.6$ V, I = 90 pA) of Cu_2Te. Inset: the corresponding FFT pattern. (g) Line profile of Cu_2Te along the blue line marked in (f), revealing the periodicity of ∼0.45 nm. (h) Typical *dI/dV* spectrum (Setpoint: $V_{bias} = 0.6$ V, I = 80 pA) of Cu_2Te marked in (e) revealing a bandgap of ∼0.3 eV. Inset: the same spectrum as (h) plotted with a logarithmic scale of the *y* axis and a smaller linear scale of the *x* axis. The positions of the valence band maximum (VBM) and conduction band minimum (CBM) are marked by "V" and "C," respectively. (i) Schematic diagram of the fabrication process. (j) and (k) Large-scale STM topographic images ($V_{bias} = 1.4$ V, I = 80 pA) of germanium deposited on Cu_2Te_2 and Cu_2Te substrates held at ∼570 K for 20 min. Inset: height profile of Ge islands. (l) Large-scale STM topographic image ($V_{bias} = 1.4$ V, I = 80 pA) of germanium deposited on Cu_2Te substrate held at ∼570 K for 40 min. Inset: height profile of the Ge film.

The terrace height of the germanium film, shown in Fig. 2(a), was measured as ∼3.7 Å. As plotted in the inset of Fig. 2(b), the high-resolution STM image demonstrates the germanium films warped with a height fluctuation of ∼25 pm, indicating minor stress between the germanium film and the substrate. As can be seen from Fig. 2(c), this germanium film exhibits the close-packed hexagonal arrangement. To rule out the possibility of bulk Ge(111) with lateral lattice constant ∼4.0 Å, a small sample bias of 325 mV was applied during the scanning process, and the honeycomb arrangement with low-buckled atomic structure was revealed [Fig. 2(d)]. The surface periodicity given by the distance between the two neighboring buckled Ge atoms [marked with red dots in Figs. 2(d) and 2(f)] is ∼0.39 nm [Fig. 2(e)], which is in good agreement with the lattice constant of freestanding germanene of 3.97–4.06 Å in the previous calculations.[31] Further analysis of the honeycomb structure [Figs. 2(d) and 2(f)] suggests a buckling height difference of ∼15 pm, confirming that the observation corresponds to buckled germanene (BG) on the Cu_2Te substrate. The proposed top and side views of the BG model are depicted in Fig. 2(g). The electronic properties of BG were analyzed by STS measurements, and the dI/dV spectra reveal a V-shaped density of states [Fig. 2(h)], a clear hallmark of the 2D Dirac system.[20] Note that since the STS spectra are recorded at room temperature, the V-shaped *dI/dV* curve is a bit rounded near the Dirac point.

With advancements in technology, the *dI/dV* spectra measured on the semiconductor substrates can quantitatively provide the dispersion information of the Dirac material, particularly Fermi velocity.[32] To determine this, we performed curve fitting based on the method described in Ref. 33, applying a work function of 3.75 eV for germanene, 4.42 eV for Cu_2Te, and 4.85 eV for Pt/It tip [Fig. 3(a)].[34,35] Accurate measurement of the tip-sample distance is essential, and to achieve this, we conducted *I/Z* spectral measurements using varying current and voltage setpoints [Fig. 3(b)]. By combining these results with the differential conductance data, we determined the tip-sample distance in this work to be 0.625 nm. To minimize the influence on the electronic band structure of the underlying substrate, it is critical that we limit our measurements and analysis to the bandgap region of the Cu_2Te substrate, which ranges from about −0.01 to 0.29 eV [Fig. 3(c)]. For this, the Fermi velocity of germanene was obtained to be (6.9 ± 0.1) × 10^5 m/s, in agreement with the previous findings.[33,36] Note that, the fitting value b is given by $b = \frac{\sqrt{2m}}{\hbar} z_0 \frac{\left(1+\frac{4\pi\hbar}{3mav_F}\right)e}{\sqrt{\bar{\varnothing}+\frac{eV_S}{2}+\frac{\hbar^2}{2m}\left(\frac{4\pi}{3a}\right)^2}}$.[33] The Fermi velocity of Dirac fermions was found to be inversely

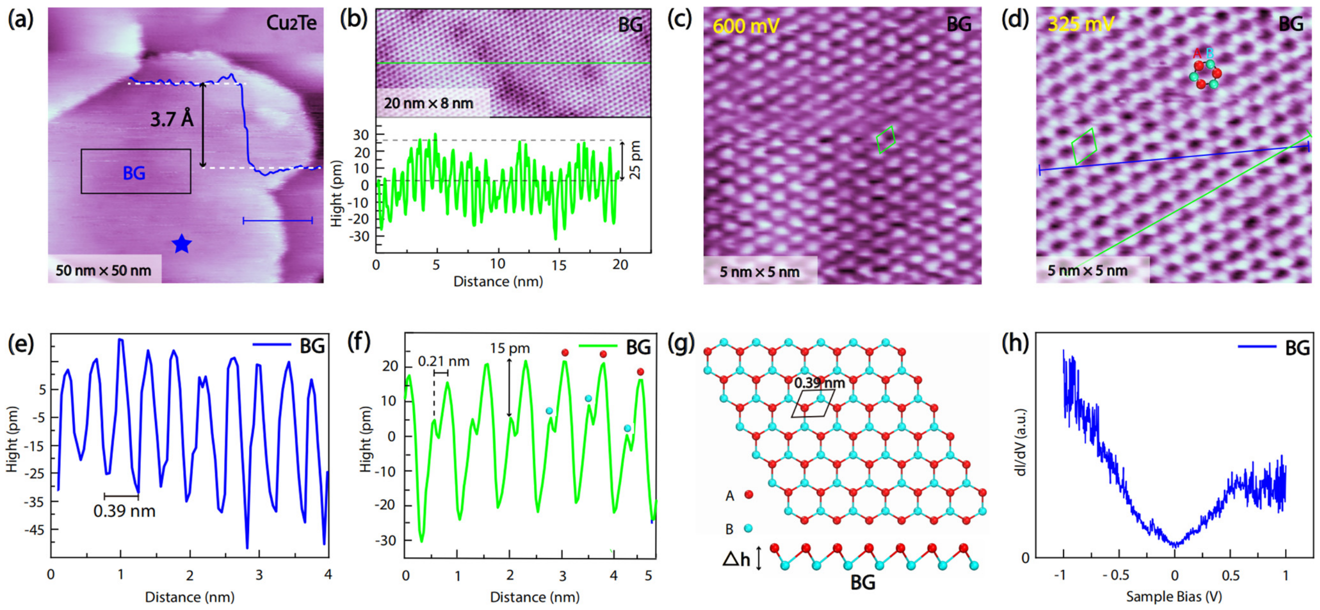

FIG. 2. Epitaxial growth of germanene on Cu_2Te. (a) Large-scale STM topographic image ($V_{bias} = 0.6$ V, I = 80 pA) of germanene film on Cu_2Te. The inset height profile shows that the step height of the film is ∼3.7 Å. (b) Upper panel: enlarged view of STM image ($V_{bias} = 0.325$ V, I = 100 pA) of germanene film, revealing the influence of surface stress. Lower panel: line profile taken along the green lines in (b), illustrating the warping of the germanene film. (c) Atomic resolution STM image ($V_{bias} = 0.6$ V, I = 80 pA) of germanene with a hexagonal lattice. (d) Atomic resolution STM image ($V_{bias} = 0.325$ V, I = 80 pA) of germanene with a honeycomb lattice. (e) and (f) Line profiles of honeycomb germanene from (d) with a lattice constant of 0.39 nm and buckling of ∼0.15 pm. (g) Ball and stick model of germanene crystalline structure (upper panel: top view, lower panel: side view). (h) The dI/dV spectrum (Setpoint: $V_{bias} = 0.6$ V, I = 80 pA) of germanene from (a) with a well-defined V shape.

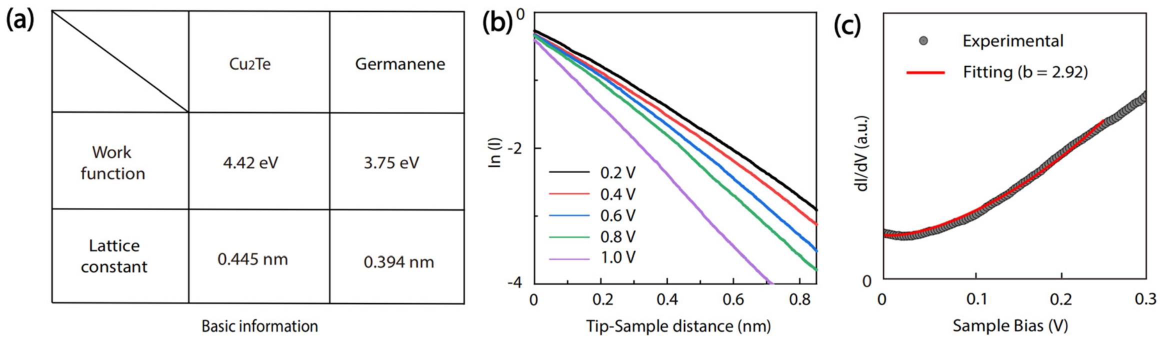

	Cu2Te	Germanene
Work function	4.42 eV	3.75 eV
Lattice constant	0.445 nm	0.394 nm

FIG. 3. (a) The adopted work function and lattice constant of Cu_2Te and germanene. (b) The relationship between the tip-sample distance and tunnel current. (c) Experimental and fitted *dI/dV* spectra of germanene, the fitting value b = 2.92, Fermi velocity $v_F = (6.9 \pm 0.1) \times 10^5$ m/s.

proportional to the dielectric constant of the supporting substrate and could be obtained by DFT calculations described previously,[37] yielding a value of 4.6×10^5 m/s. The experimentally fitting value is slightly higher than the calculated one, in essence, implying the weak coupling of germanene with the Cu_2Te substrate.

To confirm and complement the experimental results better, we conducted first-principles calculations to explore the impact of the buffer layer on the electronic structure of germanene. Because 2×2 germanene is commensurate to $\sqrt{3} \times \sqrt{3}$ Cu_2Te lattice, with a lattice mismatch of less than 1.5%. We have considered three typical configurations from possible types [see Fig. 4(a) and Fig. S4]: the Ge atom is on the bridge, hollow, and top positions of the Cu_2Te lattice, respectively. We have reached two distinct stable structures by the formation energy of germanene, which are the bridge and hollow configurations. Among them, the structure of the relaxation hollow is the same as that of the top configuration. The interlayer distance of 3.30 Å agrees with the experimental findings and further indicates the nature of van der Waals interaction between germanene and Cu_2Te.

In order to quantify the strength of the interface interaction between germanene and Cu_2Te, we identified chemically bonded atom pairs via electron localization function (ELF) analysis. It is defined as ELF = 1/[1 + (D/D_h)], where $D = \frac{1}{2}\sum_i |\nabla\varphi_i|^2 - \frac{1}{8}\frac{|\nabla\rho|^2}{\rho}$ and $D_h = \frac{3}{10}(3\pi^2\rho)^{5/3}$, where φ_i denotes the Kohn–Sham orbitals and $\rho = \sum_i |\varphi_i|^2$ represents electron charge density. The ELF values range

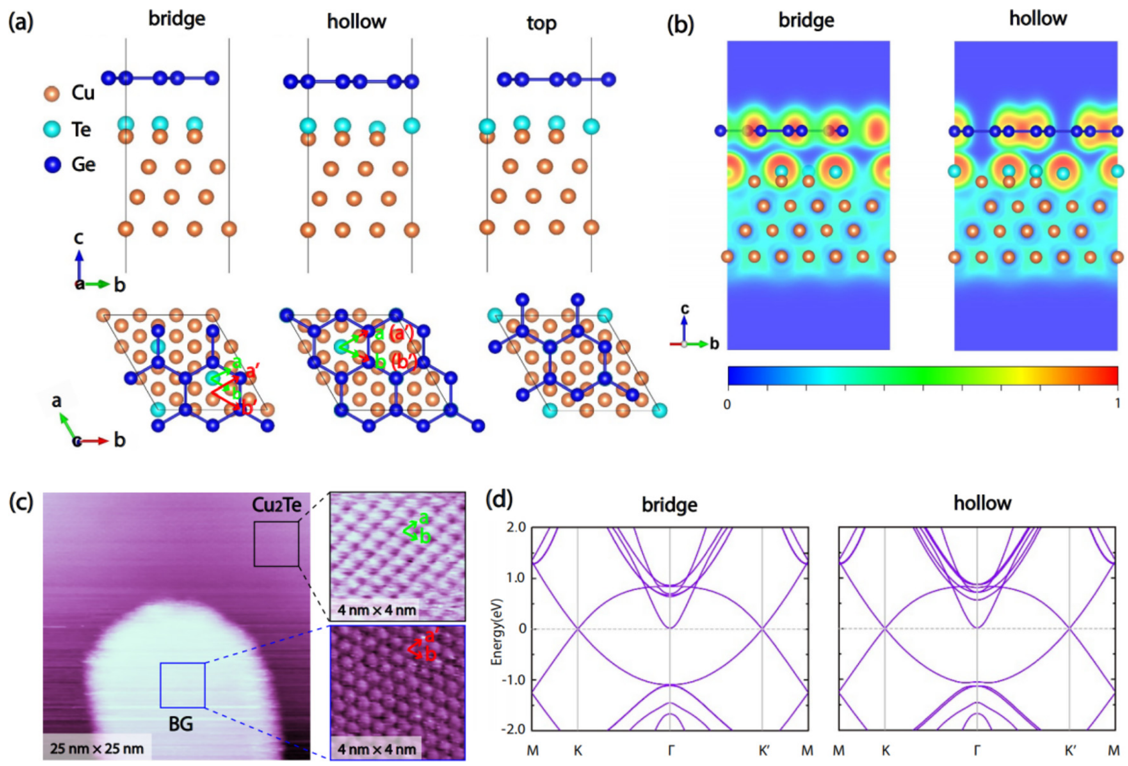

FIG. 4. Van der Waals epitaxy of germanene on semiconducting Cu_2Te. (a) Three typical configurations of germanene on Cu_2Te. (b) Electron localization function (ELF) of germanene on Cu_2Te. Left panel: the bridge configuration. Right panel: the hollow configuration. The ELF scale spans in the [0, 1] range and increases from blue to red. The blue means the formation of weak chemical bond, while the red indicates the formation of strong chemical bond. (c) Large-scale STM topographic image of germanene island surrounded by Cu_2Te. Upper panel: zoom-in STM image of Cu_2Te. Lower panel: zoom-in STM image of germanene ($V_{bias} = 0.6$ V, $I = 80$ pA). (d) Band structures of germanene detached from Cu_2Te for bridge and hollow configurations, respectively.

from 0 to 1, with ELF = 0.5 standing for the same level of Pauli repulsion as a homogeneous electron gas, while higher ELF values represent stronger electron localization. ELF = 1 corresponds to complete localization of electrons and is often associated with strong covalent interactions. As shown in Fig. 4(b), the ELF values between germanene and Cu_2Te are lower than 0.3, indicating weak van der Waals interfacial interactions. While lattice mismatch and rotational misalignment between the germanene layer and the buffer layer can lead to variations in topographic appearances (such as a moiré superstructure), our STM data reveal that the morphologies of germanene and Cu_2Te are independent of lattice orientation. Figure 4(c) schematizes the corresponding structure and the arrangement of the germanene with respect to Cu_2Te, where they share the same lattice orientation. Comparing the two types of configurations, we can determine the stable structure of germanene is the hollow configurations. Figure 4(d) presents the band structures of different configurations of germanene along the M–Γ–K–M path with spin–orbit coupling (SOC), respectively. In addition to the π bands forming a Dirac cone in the vicinity of the K point, linear Dirac bands appear close to the Fermi energy. The key difference between the two band structures is that SOC opens a small topological gap in the hollow structure.

In summary, we synthesized monolayer germanene with a low-buckled honeycomb structure through van der Waals epitaxy on semiconducting Cu_2Te. Theoretical simulations and STM measurements distinctly confirm that germanene atoms occupy threefold hollow sites of Cu_2Te, stabilized via van der Waals interaction. The Fermi velocity of $(6.9 \pm 0.1) \times 10^5$ m/s deduced from experimental dI/dV spectra fitting is slightly higher than the DFT calculated 4.6×10^5 m/s when considering the dielectric constant of the underlying Cu_2Te, demonstrating the weak coupling of germanene with the Cu_2Te substrate. The experimental realization of quasi-freestanding monolayer germanene with Dirac electronic properties opens avenues for further fundamental studies and ballistic charge transport applications.

See the supplementary material for details on extra experimental data of this work.

This work was supported by the National Natural Science Foundation of China (Grant Nos. 12174096, 51972106, 12204164, 12004295, and 12174095), the Strategic Priority Research Program of Chinese Academy of Sciences (Grant No. XDB30000000), and the Natural Science Foundation of Hunan Province, China (Grant No. 2021JJ20026). Z.J. thanks the China Postdoctoral Science Foundation (No. 2023M742900), the Postdoctoral Fellowship Program of China Postdoctoral Science Foundation (No. CZC20232196), the open Program of State Key Laboratory Silicon and Advanced Semiconductor Materials (No. SKL2023-10), and the

Fundamental Research Funds for the Central Universities (No. 2682024CX016). P.L. thanks China's Postdoctoral Science Foundation (No. 2022M722547).

AUTHOR DECLARATIONS

Conflict of Interest

The authors have no conflicts to disclose.

Author Contributions

Bo Li, Zhen Jiao, and Ping Li contributed equally to this work.

Bo Li: Conceptualization (equal); Investigation (lead); Methodology (lead); Writing – original draft (equal). **Zhen Jiao:** Data curation (equal); Formal analysis (equal); Investigation (equal); Methodology (equal); Software (equal); Writing – original draft (equal); Writing – review & editing (equal). **Ping Li:** Investigation (equal); Methodology (equal); Writing – original draft (equal). **Yanlin Tao:** Investigation (equal); Software (equal). **Qin Liao:** Investigation (supporting). **Shicheng Xu:** Investigation (supporting). **Qiwei Tian:** Investigation (supporting). **Chen Zhang:** Investigation (supporting). **Li Zhang:** Investigation (supporting). **Yuan Tian:** Investigation (supporting). **Long-Jing Yin:** Investigation (supporting). **Lijie Zhang:** Conceptualization (equal); Formal analysis (equal); Investigation (equal); Supervision (equal); Writing – original draft (lead); Writing – review & editing (equal). **Zhihui Qin:** Conceptualization (equal); Funding acquisition (lead); Investigation (equal); Project administration (lead); Resources (lead); Supervision (lead); Writing – original draft (equal); Writing – review & editing (lead).

DATA AVAILABILITY

The data that support the findings of this study are available from the corresponding author upon reasonable request.

REFERENCES

[1] K. S. Novoselov, A. K. Geim, S. V. Morozov, D. Jiang, Y. Zhang, S. V. Dubonos, I. V. Grigorieva, and A. A. Firsov, Science **306**, 666 (2004).

[2] A. H. Castro Neto, F. Guinea, N. M. R. Peres, K. S. Novoselov, and A. K. Geim, Rev. Mod. Phys. **81**, 109 (2009).

[3] S. B. Desai, S. R. Madhvapathy, A. B. Sachid, J. P. Llinas, Q. Wang, G. H. Ahn, G. Pitner, M. J. Kim, J. Bokor, C. Hu, H. S. P. Wong, and A. Javey, Science **354**, 99 (2016).

[4] K. S. Novoselov, A. Mishchenko, A. Carvalho, and A. H. Castro Neto, Science **353**, aac9439 (2016).

[5] B. Li, M. Bagheri Tagani, S. Izadi Vishkayi, Y. Yang, J. Wang, Q. Tian, C. Zhang, L. Zhang, L.-J. Yin, Y. Tian, L. Zhang, and Z. Qin, Appl. Phys. Lett. **122**, 031902 (2023).

[6] A. Acun, L. Zhang, P. Bampoulis, M. Farmanbar, A. van Houselt, A. Rudenko, M. Lingenfelder, G. Brocks, B. Poelsema, M. I. Katsnelson, and H. J. W. Zandvliet, J. Phys.: Condens. Matter **27**, 443002 (2015).

[7] Q. Yao, L. Zhang, N. S. Kabanov, A. N. Rudenko, T. Arjmand, H. Rahimpour Soleimani, A. L. Klavsyuk, and H. J. W. Zandvliet, Appl. Phys. Lett. **112**, 171607 (2018).

[8] Q. Wu, M. Bagheri Tagani, Q. Tian, S. Izadi Vishkayi, L. Zhang, L.-J. Yin, Y. Tian, L. Zhang, and Z. Qin, Appl. Phys. Lett. **121**, 051901 (2022).

[9] Z. Ni, Q. Liu, K. Tang, J. Zheng, J. Zhou, R. Qin, Z. Gao, D. Yu, and J. Lu, Nano Lett. **12**, 113 (2012).

[10] C. C. Liu, W. X. Feng, and Y. G. Yao, Phys. Rev. Lett. **107**, 076802 (2011).

[11] P. Bampoulis, C. Castenmiller, D. J. Klaassen, J. van Mil, Y. Liu, C.-C. Liu, Y. Yao, M. Ezawa, A. N. Rudenko, and H. J. W. Zandvliet, Phys. Rev. Lett. **130**, 196401 (2023).

[12] L. Li, S.-Z. Lu, J. Pan, Z. Qin, Y.-Q. Wang, Y. Wang, G.-Y. Cao, S. Du, and H.-J. Gao, Adv. Mater. **26**, 4820 (2014).

[13] M. E. Davila, L. Xian, S. Cahangirov, A. Rubio, and G. Le Lay, New J. Phys. **16**, 095002 (2014).

[14] P. Bampoulis, L. Zhang, A. Safaei, R. van Gastel, B. Poelsema, and H. J. W. Zandvliet, J. Phys.: Condens. Matter **26**, 442001 (2014).

[15] M. Derivaz, D. Dentel, R. Stephan, M.-C. Hanf, A. Mehdaoui, P. Sonnet, and C. Pirri, Nano Lett. **15**, 2510 (2015).

[16] J. Gou, Q. Zhong, S. Sheng, W. Li, P. Cheng, H. Li, L. Chen, and K. Wu, 2D Mater. **3**, 045005 (2016).

[17] Z. Qin, J. Pan, S. Lu, S. Yan, Y. Wang, S. Du, H.-J. Gao, and G. Cao, Adv. Mater. **29**, 1606046 (2017).

[18] C.-H. Lin, A. Huang, W. W. Pai, W.-C. Chen, T.-Y. Chen, T.-R. Chang, R. Yukawa, C.-M. Cheng, C.-Y. Mou, I. Matsuda, T. C. Chiang, H. T. Jeng, and S. J. Tang, Phys. Rev. Mater. **2**, 024003 (2018).

[19] Q. Tian, X. Guo, S. Izadi Vishkayi, M. Bagheri Tagani, L. Zhang, Y. Tian, L.-J. Yin, H. Huang, L. Zhang, and Z. Qin, Phys. Rev. B **110**, 125430 (2024).

[20] L. Zhang, P. Bampoulis, A. N. Rudenko, Q. Yao, A. van Houselt, B. Poelsema, M. I. Katsnelson, and H. J. W. Zandvliet, Phys. Rev. Lett. **116**, 256804 (2016).

[21] J. Zhuang, C. Liu, Z. Zhou, G. Casillas, H. Feng, X. Xu, J. Wang, W. Hao, X. Wang, S. X. Dou, Z. Hu, and Y. Du, Adv. Sci. **5**, 1800207 (2018).

[22] I. Horcas, R. Fernández, J. Gomez-Rodriguez, J. Colchero, J. Gómez-Herrero, and A. Baro, Rev. Sci. Instrum. **78**, 013705 (2007).

[23] J. P. Perdew, K. Burke, and M. Ernzerhof, Phys. Rev. Lett. **77**, 3865 (1996).

[24] M. Dion, H. Rydberg, E. Schroder, D. C. Langreth, and B. I. Lundqvist, Phys. Rev. Lett. **92**, 246401 (2004).

[25] H. J. Monkhorst and J. D. Pack, Phys. Rev. B **13**, 5188 (1976).

[26] T. Kiβlinger, A. Raabgrund, B. Geldiyev, M. Ammon, J. Rieger, J. Hauner, L. Hammer, T. Fauster, and M. A. Schneider, Phys. Rev. B **102**, 155422 (2020).

[27] T. Kiβlinger, M. A. Schneider, and L. Hammer, Phys. Rev. B **104**, 155426 (2021).

[28] K. Qian, L. Gao, X. Chen, H. Li, S. Zhang, X.-L. Zhang, S. Zhu, J. Yan, D. Bao, L. Cao, J.-A. Shi, J. Lu, C. Liu, J. Wang, T. Qian, H. Ding, L. Gu, W. Zhou, Y.-Y. Zhang, X. Lin, S. Du, M. Ouyang, S. T. Pantelides, and H.-J. Gao, Adv. Mater. **32**, 1908314 (2020).

[29] Y. F. Tong, M. Bouaziz, W. Zhang, B. Obeid, A. Loncle, H. Oughaddou, H. Enriquez, K. Chaouchi, V. Esaulov, Z. S. Chen, H. Q. Xiong, Y. C. Cheng, and A. Bendounan, 2D Mater. **7**, 035010 (2020).

[30] J. Feng, H. Gao, T. Li, X. Tan, P. Xu, M. Li, L. He, and D. Ma, ACS Nano **15**, 3415 (2021).

[31] S. Cahangirov, M. Topsakal, E. Akturk, H. Sahin, and S. Ciraci, Phys. Rev. Lett. **102**, 236804 (2009).

[32] Z. Jiao and H. J. W. Zandvliet, Appl. Phys. Lett. **118**, 163103 (2021).

[33] H. J. W. Zandvliet, Q. Yao, L. Zhang, P. Bampoulis, and Z. Jiao, Phys. Rev. B **106**, 085423 (2022).

[34] B. Borca, C. Castenmiller, M. Tsvetanova, K. Sotthewes, A. N. Rudenko, and H. J. W. Zandvliet, 2D Mater. **7**, 035021 (2020).

[35] J. Park, J. Seo, J. H. Lim, and B. Yoo, Front. Chem. **10**, 799305 (2022).

[36] M. E. Dávila and G. L. Lay, Sci. Rep. **6**, 20714 (2016).

[37] P. Li, J. Cao, and Z.-X. Guo, J. Mater. Chem. C **4**, 1736 (2016).